A Computational Model of Nanoparticle Growth

from spark ablation in the gas phase

B.E. van der Maesen

Thesis Committee:	Dr. ir. M.B. van Gijzen	TU Delft
	Prof. dr. ir. A.W. Heemink	TU Delft
	Dr. M. Boeije	VSPARTICLE

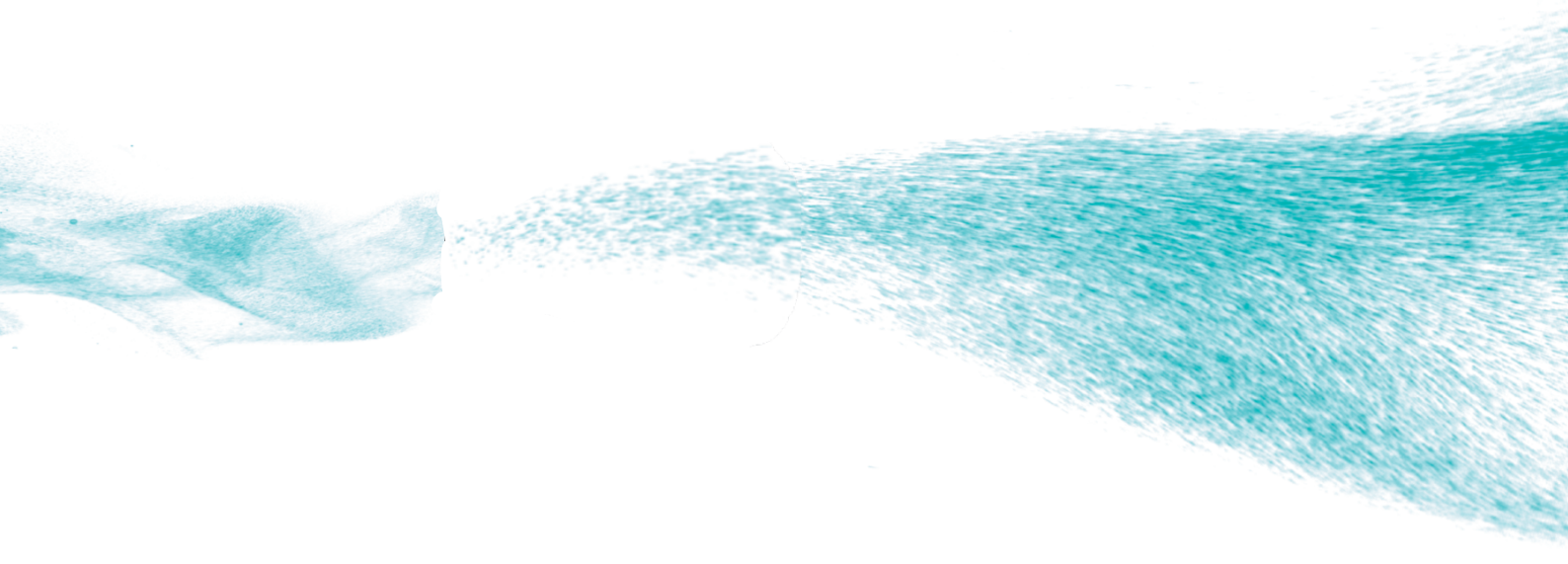

TU Delft Delft University of Technology

Challenge the future

A Computational Model of Nanoparticle Growth

from spark ablation in the gas phase

by

B.E. van der Maesen

Literature Study prior to the fulfillment of a thesis in

in Applied Mathematics

at the Delft University of Technology.

Thesis committee:	Dr. ir. M. B. van Gijzen,	TU Delft
	Prof. Dr. ir. A. W. Heemink,	TU Delft
	Dr. ir. M. Boeije,	VSPARTICLE

TU Delft Delft University of Technology

Contents

List of Figures

List of Symbols & Constants

Quantity	Symbol	Unit	Value
Elementary Quantities			
Length	L , l	meter, m or nanometer, nm	
Mass	m	kilogram, kg	
Time	t	second, s or millisecond, ms	
Pressure	P	Pascal, Pa	
Temperature	T	Kelvin, K	
Spacial coordinate	x	m	
Volume space	V	m^3	
Density	ρ	kg/m^3	
Viscosity	μ	$Pa \cdot s$	
Activation energy	E	J	
Inflow	Q	$m^3 s^{-1}$	
Molecular mass	m_m	kg/mol	
diameter	d	m	
radius	r	m	
Defined Quantities			
particle volume	v	m^3	
ablation power	P_A	W	
spark frequency	f	s^{-1}	
number particle concentration	N, n	–	
gas mean free path	λ	m	
Collision frequency kernel free molecular	β_F	$m^{5/2} s^{-1}$	
Collision frequency kernel continuum	β_{Co}	$m^3 s^{-1}$	
Coagulation constant free molecular	K_F	$m^{5/2} s^{-1}$	
Coagulation constant continuum	K_{Co}	$m^3 s^{-1}$	
Knudsen number	Kn	–	
Cunningham Slip Correction factor	$C(v)$	–	
Gas Constant	$R_g = \frac{Pv}{nT}$	$J/mol \cdot K$	
Mass fractal dimension	D_f	–	
Geometric standard deviation w.r.t. particle size	σ	–	
dimensionless particle size distribution	φ, $\frac{n(v)v}{N}$	–	
Total number of residence times	$\tilde{N} = \frac{t_{\mathrm{TOTAL}}}{t_R}$	–	
k-th Moment	M_k	m^{3k}	
geometric mean particle size	v_g	m^3	
Constants			
Boltzmann constant	k_B	$m^2 kg/s^2 K$	$1.380\,648\,52 \times 10^{-23}$
Avogadro's number	N_A	$atoms\,mol^{-1}$	$6.022\,140\,9 \times 10^{23}$

1

INTRODUCTION

Nanoscience is the field of research that allows scientists to observe, study and manipulate the smallest building blocks of every physical aspect on Earth: nanoparticles. Nanoparticles range from 1 to 100 nm in size and consist of (a combination of) (in)organic molecules. To compare, the typical size of a nanoparticle to a football, is as a football to the Earth (Figure 1.1). Materials at this scale obtain different physical properties like electric charge, color, and viscosity, than they experience in bulk form. The ability to control these properties at nanoscale will allow the development of new materials with countless applications. Although nanotechnology is a relatively new field of research, it has rapidly become indispensable for innovation in sectors like sustainable energy, medicine and electronics.

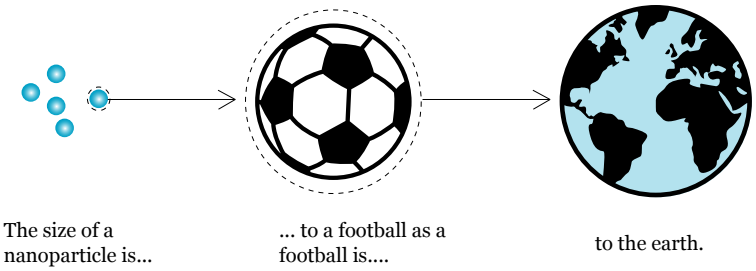

Figure 1.1: Nanoparticle size on a comparative scale.

The production of nanoparticles is required for research in the field of nanotechnology. VSPARTICLE sidelines the original, complex and time consuming method using liquid chemicals, with a new and easy nanoparticle production system: the VSP-G1. This system uses a gas phase physical process called spark ablation. The material is heated shortly to an extremely high temperature causing the material to evaporate to a highly concentrated aerosol. The aerosol is transported through a tube allowing particles to collide and grow. Lastly,the nanoparticles are deposited onto a substrate.

VSPARTICLE aims for a highly efficient and fully controllable system generating nanoparticles of any desired quantity, particle size and shape. A computational model of the nanoparticle production process is required to achieve an entire understanding with respect to the system, the output and the corresponding parameter sensitivity. It will contribute significantly to a completely controllable VSP-G1 system. This literature study provides the theoretical groundwork necessary to construct such a computational model, describing the transport of aerosol and nanoparticle growth in the VSP-G1 in particular. Smoluchowski [7] developed a population balance equation which mathematically describes aerosol dynamics, forming the foundation of this present study.

The physical aspects of the VSP-G1, with emphasis on aerosol transport, is provided in the current chapter. Chapter two provides extensive theory on aerosol dynamics and nanoparticle growth due to Brownian Motion in particular. The physical properties of the VSP-G1 and the mathematical description of aerosol dynamics are used to develop a basic model in Chapter three. Using the log-normal method of moments solution method the model is implemented in Chapter four, and a reflection is given on the first results. Lastly, chapter five concludes with findings from the present study and states preliminary research questions and goals for the remainder of this thesis.

1.1. VSP-G1

The production of tailor-made nanoparticles is traditionally performed by wet-chemistry techniques, often leading to material impurities and production wastes. In contrast, a gas-phased technique like the method of the VSP-G1, guarantees a user-friendly and fast production of ultra pure nanoparticles. The production process consists of three phases.

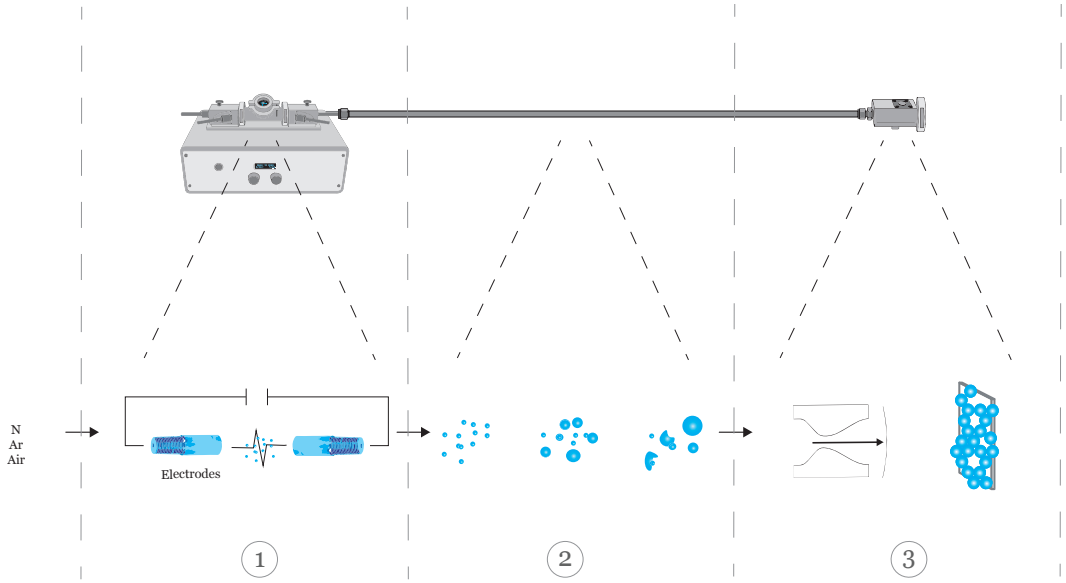

Figure 1.2: Nanoparticle production process of the VSP-G1

A physical description of the VSP-G1 and the corresponding set up is given in figure 1.2.

First, a potential difference causes a spark which locally vaporizes the bulk material of the electrodes. The resulting plasma has a temperature of order 10^4 K, and therefore is in the gas phase, containing individual atoms [8]. Almost instantly after, the vapor blends with a continuous flow of carrier gas, which is channeled through the electrodes. The gas has a controllable temperature of around of 296.15 K and is either composed of nitrogen, argon or air. The sudden drop in temperature causes the material to condensate, producing an aerosol of pure nanoparticles [9] with a certain starting concentration N_0.

Transport of aerosol through a tube is the second phase and allows nanoparticles to interact due to Brownian Motion [8]. When two or more particles collide they either fuse into one larger spherical particle or (loosely) stick together to form a non-spherical agglomerate. Particle growth is dependent on various parameters. A computational model simulating this phase will provide a parameters sensitivity analysis with respect to the particles final size and shape and therefore contribute to the production of pure, tailor-made nanoparticles.

The last phase consists of three possible methods to deposit nanoparticles onto a substrate. A diffusion chamber lets particles randomly diffuse onto a surface, creating a smooth coating used for instance for the development of microchips. Impaction, visualized in figure 1.2, is another technique that accelerates a stream of particles through a nozzle, literately "impacting" on the substrate and making exact positioning of particles possible. Lastly, it is also possible to deposit particles of a certain size range by applying a filter with a corresponding mesh size.

1.2. GOAL

The aim of this literature study is to support the development of a numerical and computationally efficient model of phase two of the nanoproduction process: nanoparticle growth during aerosol transport. Such a model is generated by taking the following steps:

1. Define the physical aspects of nanoparticle growth in the VSP-G1.
2. Define a corresponding mathematical description to construct a mathematical model.
3. Identify the most feasible solution method.
4. Develop a computational model, and generate results.
5. Expand the model to improve accuracy and efficiency.

This report treats steps 1-4 for nanoparticle growth in the VSP-G1 under the most basic conditions: purely spherical growth in a closed space. The present study concludes by reflecting on the current model, recommending feasible expansions and looking into future possibilities with respect to this master thesis.

1.3. LITERATURE OVERVIEW

An overview of the general properties, behaviour and measurement of airborne particles is given by Hinds [10] and Hampden-Smith [2], providing the theoretical fundamentals of aerosol dynamics.

Nanoparticle growth due to coagulation, a growth mechanism caused by collision and fusion of particles, was first mathematically described by a population balance equation in 1916, and was named after Marion Smoluchowski [7]. Twelve years later the original Smoluchowski equation was expanded by Müller [11], incorporating the Navier Stokes equations and taking other growth mechanisms into account [12]. The expression for aerosol dynamics still had limitations with respect to the solid- and gas particle size ratio. Fuchs overcame this in 1970, by deriving the Smoluchowski equation for the entire particle size range.

A wide range of publications focus on different solution methods for the population balance equation in terms of particle number concentration. Lee (1983) [5] provided an analytical solution for the Smoluchowski equation based on an integration of the method of moments and a log-normal approximation of the solution, the so called "log-normal method of moments", which is the technique used in the present study. The further development the method of moments, is given by Yu and Yueyan [12]. The work of Lee, Chen and Gieseke extended Lee's previous theory and developed the solution method for the entire particle size range (1984)[32]. The present study follows this method and applies it to approximate the particle growth in the VSP-G1.

A simple model to predict the evolution of singlet nanoparticles produced by the VSP-G1 under conditions that guarantee pure spherical growth is developed by Feng [9]. Fengs model analytically solves a first-order homogeneous nonlinear ordinary differential equation, which clearly doesn't correspond to a population balance equation:

$$\frac{dN}{dt} = -\frac{1}{2}\beta N^2(t), \tag{1.1}$$

where β is a constant and $N(t)$ is the total particle number concentration.

Although there are many publications on the computational aspects of nanoparticle growth, a detailed numerical model based on the original Smoluchowski equation for approximating nanoparticle growth in the VSP-G1 has not yet been developed. Therefore, it is worth conducting research on solution methods like the log-normal method of moments to solve the Smoluchowski equation under conditions corresponding to the VSP-G1.

2

THEORY

Aerosol kinematics and dynamics is influenced by interaction between solid particles. Coagulation is an inter-particle mechanism which occurs when two particles collide and stick together to form a new, larger particle. [2]. As coagulation takes place the average particle size increases, the particle concentration of a certain aerosol sample decreases, while the total particle mass and volume stay constant. It is the most important nanoparticle growth mechanism to consider when simulating aerosol dynamics and the growth of particles in particular as it is the basis of the mathematical description of nanoparticle dynamics: the Smoluchowski equation (Section 2.1).

Coagulation is mainly driven by Brownian Motion of particles. In a homogeneous gas, Brownian Motion is the random motion of suspended particles due to their collisions with the gas particles [2]. The number of collisions between particles is given by the collision frequency kernel which depends on various aerosol properties explained in Section 2.2.

The chapter concludes with an expression for the particle size distribution describing the effect of coagulation with respect to particle size in Section 2.3.

2.1. SMOLUCHOWSKI EQUATION

The evolution of aerosol particle behaviour and properties originating from both internal and external mechanisms are described by the Smoluchowski equation. Its original form only accounts for colloid coagulation [12]. A colloid is a mixture of microscopically dispersed particles which are incapable of being dissolved and suspended with another substance. The original expression for the coagulation rate in a closed phase space is [2]:

$$\frac{\partial n(v,t)}{\partial t} = \frac{1}{2}\int_0^v \beta(v', v-v', t)n(v', t)n(v-v', t)dv' - n(v,t)\int_0^\infty \beta(v, v', t)n(v', t)dv' \tag{2.1}$$

Equation (2.1) gives the rate of change of the particle size distribution. $n(v,t)dv$ is the number of particles whose volume is between v and $v+dv$ at time t [12]. The first term on the right hand side accounts for the formation of particles of volume v, by coagulation of smaller particles. The factor $1/2$ is necessary to avoid double counting collisions. The second term accounts for the loss of particles of volume v, by coagulation with others. This is called a "population balance equation". $n(v,t)$ is the number of particles with volume v at time t. $\beta(v,v')$ is the collision frequency kernel describing the number of collisions between particles of size v and v' at time t.

The extended Smoluchowski equation accounts for almost all aerosol dynamics including external mechanisms due to aerosol transport through air [12], which introduces the spatial coordinate x, and incorporates the Navier-Stokes equation:

$$\begin{aligned}\frac{\partial n(v,x,t)}{\partial t} &+ \frac{\partial\big(un(v,x,t)\big)}{\partial x} + \frac{\partial\big(u_{th}n(v,x,t)\big)}{\partial x} \\ &= \frac{\partial}{\partial x}\Big(D_B\frac{\partial n(v,y,t)}{\partial x}\Big) + \frac{\partial\big(G_r n(v,x,t)\big)}{\partial v} + J\big(v^*,x,t\big)\delta(v-v^*) \\ &- \frac{1}{2}\int_{v^*}^{v}\beta(v',v-v',t)n(v',x,t)n(v-v',t)dv' \\ &- n(v)\int_{v^*}^{\infty}\beta(v,v',t)n(v',x,t)dv' + \int_{v}^{\infty}a(v')b(v|v')n(v',t)dv' \\ &- a(v)n(v,t) + ... \end{aligned} \tag{2.2}$$

where $n(v,x,t)$ is the particle number density for particle volume v, spatial coordinate x, and time t; the value β represents the collision frequency; u is the particle velocity, u_{th} is the velocity of particles in response the change in temperature; D_B is the Brownian diffusion coefficient; G_r is the particle surface growth rate; J is the source term, i.e. the nucleation rate of atomic-sized particles v^*; a and b are parameters accounting for the breakage of (non)-spherical particles due to shear force along the walls of the tube. [12].

The thermophoresis velocity u_{th} can be neglected considering the conditions in the VSP-G1: the aerosol obtains a constant temperature during transport. G_r can also be discarded due to its dependence on thermodynamics.

The first and simplest method for describing aerosol dynamics in the VSP-G1 of this present study develops a computational model for the original Smoluchowski equation (2.1), which accounts for coagulation in a closed space. Eventually, the model can be extended with the most impactful parts of Equation 2.2, such as the transport equation or the (continuous) nucleation of new particles.

2.2. COLLISION FREQUENCY KERNEL

The collision frequency kernel β, is dependent on the interaction between the ablated nanoparticles and the surrounding gas particles, and in particular the size ratio between the two different particles. It is necessary to introduce the mean free path λ and the Knudsen number Kn.

The gas mean free path is defined as the average distance travelled by a gas molecule between successive collisions [10]. The Knudsen number relates the gas mean free path to the particle diameter and determines in which "regime" particle motion takes place. Each regime consists of a unique expression for β.

$$Kn = \frac{2\lambda}{d_p} \tag{2.3}$$

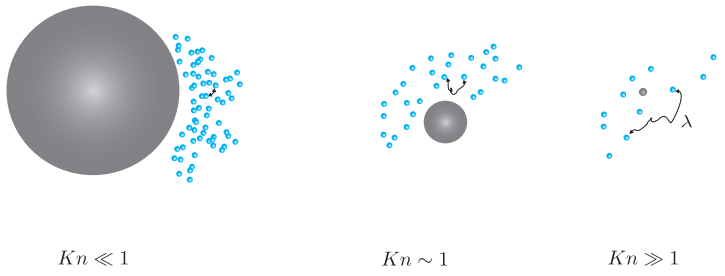

Figure 2.1: Particle dynamics in continuum, transition and free-molecular regime [1]. Note, various publications obtain different Knudsen ranges with respect the corresponding the regimes. Kodas [2] states that the the transition regime holds for $1 < Kn < 50$, while it is much lower according to Rader [3]: $0.4 < Kn < 20$.

The gas mean free path is described in terms of the particle concentration n and the gas particle diameter d_g [2]:

$$\lambda = \frac{1}{\sqrt{2} n \pi d_g^2} \tag{2.4}$$

Using the ideal gas law the particle concentration can be described as $n = \frac{N}{V} = \frac{P}{k_B T}$ and another approximation of the gas mean free path is constructed:

$$\lambda = \frac{k_B T}{\sqrt{2} \pi d_g^2 P}, \tag{2.5}$$

where k_B is the Boltzmann constant, T the temperature and P pressure.

The gas mean free path and the Knudsen number for different carrier gasses and particle diameters are defined in Table 2.1 for standard VSP-G1 conditions.[1]

Gas	λ_0 [μm]	Kn for $d_p = 1$ nm	Kn for $d_p = 5$ nm	Kn for $d_p = 10$ nm
Argon gas	0.0703	140.60	28.12	14.06
Air	0.0674	134.80	26.96	13.40
Nitrogen gas	0.0230	460.00	92.00	23.00

Table 2.1: Gas free mean path and Knudsen values for argon-, air and nitrogen gas under standard VSP-G1 conditions for three different particle sizes.

Based on the values in Table 2.1 and previous studies ([2, 3, 10, 13]), the free molecular regime is considered for the production of nanoparticles with diameters up to 5 nm. The transition regime will apply for particles exceeding this size. Although the continuum regime is not considered initially, it is treated in this present study as its properties are necessary to define the collision kernel in the transition scheme. Furthermore, the continuum regime may be applicable for the formation of agglomerates.

2.2.1. FREE MOLECULAR REGIME

In the free molecular regime, collisions take place by a ballistic process in which the particles can be treated as large molecules [2]. The collision frequency kernel is described as:

$$\beta_F(v_i, v_j) = K_F \left(\frac{3}{4\pi}\right)^{1/6} \left(\frac{1}{v_i} + \frac{1}{v_j}\right)^{1/2} \left(v_i^{1/3} + v_j^{1/3}\right)^2 \tag{2.6}$$

$$K_F = \left(\frac{6 k_B T}{\rho_g}\right)^{1/2}, \tag{2.7}$$

where v_i and v_j are particle volumes, K_F the coagulation constant for the free-molecule regime, ρ_g is the gas density in (kg/m^3), and the other parameters are previously defined. Under standard conditions[1] the densities and corresponding coagulation constants for different gas types in Table 2.2.

Gas	ρ_{g0} [kg/m^3]	K_F [m$^{5/2}$s^{-1}]
Argon gas	1.645	1.221×10^{-10}
Air	1.192	1.435×10^{-10}
Nitrogen gas	1.165	1.451×10^{-10}

Table 2.2: gas density and coagulation constants for primarily types of carrier gas used in the VSP-G1

[1] $T_0 = 296.15$ K; $P_0 = 101.325$ kPa

The *characteristic time for coagulation* defines the importance of coagulation on aerosol dynamics. It is equal to the time it takes for particles to reduce to a concentration which is half its initial value [2] and can be compared to the experimental residence time, to indicate to what extent coagulation has taken place.

$$t_{CF} \approx \left(\left(\frac{3V}{4\pi} \right)^{1/6} K_F N_0^{5/6} \right)^{-1}, \tag{2.8}$$

where V is the total particle volume fraction, N_0 the initial particle concentration and K_F defined in Equation 2.7.

2.2.2. CONTINUUM REGIME

Particles are described in the continuum regime when their size is much larger than the mean free path ($Kn \ll 1$). Collisions occur due to Brownian Motion and are described by the collision frequency kernel for the continuum regime:

$$\beta_C(v_i, v_j) = K_C \left(v_i^{1/3} + v_j^{1/3} \right) \left(\frac{1}{v_i^{1/3}} + \frac{1}{v_j^{1/3}} \right) \tag{2.9}$$

$$K_C = \frac{2 k_B T}{3\mu}, \tag{2.10}$$

where μ is the gas viscosity in [kg/ms]. Non-continuum effects start to appear as the Knudsen number reaches its upper boundary: $Kn = 0.25$ [3], [13]. To account for these effects, the Cunningham Slip Correction factor is incorporated into Equation 2.9:

$$\beta_{Co}(v_i, v_j) = K_{Co} \left(v_i^{1/3} + v_j^{1/3} \right) \left(\frac{C(v_i)}{v_i^{1/3}} + \frac{C(v_j)}{v_j^{1/3}} \right), \tag{2.11}$$

where $K_{Co} = K_C$. The characteristic time for coagulation does not apply to the present research, but the value for β_{Co} is needed in order to define the collision kernel of the transition regime in Section 2.2.3. Rader conducted research on the slip correction factor for small particles in nine common gasses [3] and found the following expression.

$$C(Kn) = 1 + Kn \left(\alpha + \beta \exp(-\gamma / Kn) \right) \tag{2.12}$$

α, β and γ are parameters that are adjusted to best fit the data and corresponding regime. Under standard conditions [1], the following values hold for the transition regime:

Transition Regime	Ar	N2	Air
α	1.227	$1.207 \pm 5\%$	1.207
β	0.42	$0.40 \pm 5\%$	0.40
γ	0.85	$0.78 \pm 5\%$	0.78

Table 2.3: Parameters for Cunningham Slip Correction factor for different gasses and regimes

2.2.3. TRANSITION REGIME

For particles with a diameter that is approximately the same as the gas mean free path ($d_p \approx \lambda$), coagulation occurs in the transition regime. Different methods exists to combine β_F and β_{Co} to approximate the transition kernel.

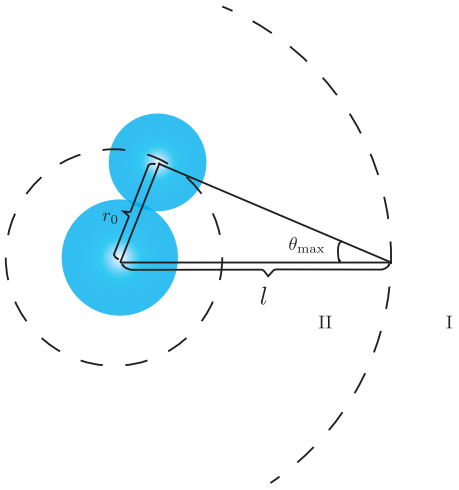

Figure 2.2: Geometry of the collision model in the flux matching method [4]

Fuchs developed the flux matching method to combine the free - molecular and continuum kernel to form the transition kernel [14]. The method assumes that outside a distance l, from the center of one of the colliding particles, the diffusion theory is considered and fluxes are described as they are in the continuum regime, (area I in Figure 2.2). Within the distance l, particle fluxes are considered by the kinetic gas theory [15], (area II). Fluxes are matched at the distance l. The location of the boundary varies per method. The present research investigates the most basic method: the harmonic mean, and Dahneke (1983)'s method, which is also known for its accuracy and simplicity [14].

The harmonic mean matches the fluxes at the collision sphere [14], which is the distance between the centers of two particles at the moment of collision ($r_1 + r_2$). The collision frequency kernel following the harmonic mean method is equal to [15]:

$$\beta_{T_h} = \left(\frac{1}{\beta_{Co}(v_i, v_j)} + \frac{1}{\beta_F(v_i, v_j)} \right)^{-1} \tag{2.13}$$

Dahneke describes the diffusion as a mean free path phenomenon [14] and matches the two fluxes at a distance equal to the mean free path of the particles. In the literature Dahneke's kernel β_{T_D} is preferred because of its accuracy relative to the harmonic mean, but also for its simplicity in respect to other methods found by Fuchs and Wright [13], [14], [15]:

$$\beta_{T_D} = \beta_{Co} \frac{1 + Kn_D}{1 + 2Kn_D + 2Kn_D^2}, \tag{2.14}$$

$$Kn_D = \frac{\beta_{Co}(v_i, v_j)}{2\beta_F(v_i, v_j)}$$

2.2.4. AGGLOMERATE KERNEL

If two solid particles collide, the result may be an agglomerate or a spherical particle, depending on the relative rates of fusion and collision. An agglomerate is a particle formed by two or more smaller particles which have not fully fused into a sphere [2]. The mechanism that causes two particles to fuse is called sintering. The rate of sintering is a strong function of temperature, particle size and material properties. When the characteristic time for sintering t_S is greater than the characteristic collision time t_C, an agglomerate forms instead of a spherical particle.

$$t_S = A d_p^4 \exp\left(\frac{E}{R_g T}\right) \tag{2.15}$$

Where E is the activation energy for diffusion, R_g is the gas constant and A is a constant.

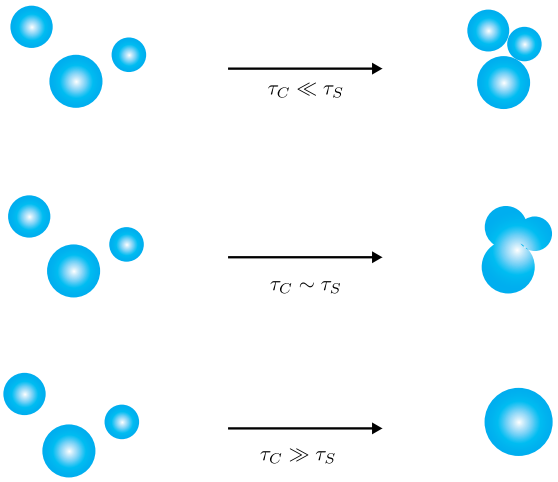

Figure 2.3: Particle morphologies v.s. collision rate [2]

The transport properties of agglomerates are substantially different from spherical primary particle properties. The *mass fractal dimension*, D_f defines the irregular structure of the agglomerates in terms of its "openness" [2]. Typically D_f varies from 1 to 3. $D_f = 3$ defines a solid sphere, while $D_f = 1$ corresponds with primary particles stuck together in a single line. According to previous research [9], the VSP-G1 creates agglomerates with a fractal dimension between $1.7 < D_f < 2.2$.

The expression for the collision frequency kernel of agglomerates in the free-molecular regime varies slightly from its expression for spherical particles (Equation 2.6):

$$\beta_{FA}(v_i, v_j) = K_F \left(\frac{3}{4\pi}\right)^{1/6} \left(\frac{1}{v_i} + \frac{1}{v_j}\right)^{1/2} \left(v_i^{1/D_f} + v_j^{1/D_f}\right)^2 \tag{2.16}$$

However, according to [2] this equation is limited to $D_f \geq 2$.

Further research regarding agglomeration is required in order to implement this mechanism into the computational model. An accurate mathematical description is needed for agglomerates with $D_f \leq 2$, as well as the formation of agglomerates in the transition regime.

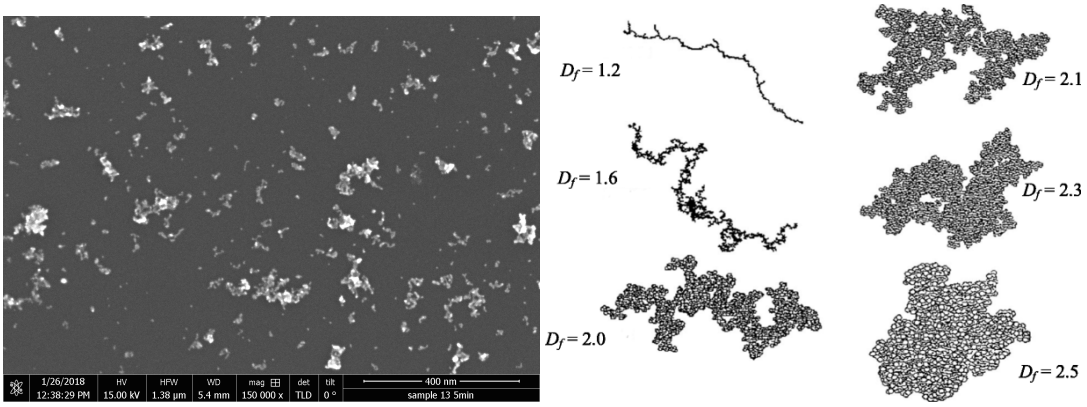

(a) Picture of agglomerates taken from the VSP-G1 after deposition

(b) Fractal dimension D_f corresponding with the irregular structure of agglomerates [16]

Figure 2.4: Agglomerate structures

2.3. SELF-PRESERVING SIZE DISTRIBUTION

Coagulation of nanoparticles is described by the particle number concentration and size change as a function of time [10]. The particle size concentration (PSD) $n(v,t)$, is obtained by solving the Smoluchowski equation.

When coagulation occurs in a closed space, it is possible to write the PSD in dimensionless form [2], becoming invariant with respect to time. The dimensionless PSD approaches a log-normal distribution with a constant geometric standard deviation $\sigma_\infty = 1.355$ as $t \to \infty$. The so called *self-preserving size distribution (SPSD)* is a function of the dimensionless volume $\eta = \frac{v}{v_g}$ and is log-normal with a geometric standard deviation σ_∞:

$$\varphi(\eta) = \frac{n(v)v}{N} = \frac{1}{3\sqrt{2\pi}\ln\sigma_\infty} \exp\left[\frac{-\ln^2(\eta)}{18\ln^2(\sigma_\infty)}\right], \tag{2.17}$$

where v_g is the geometric mean particle volume and N the total particle concentration. The time required to reach the SPSD is dependent on the dispersity of the initial size distribution and particle concentration. SPSDs for charged particles are generally much narrower than those obtained with uncharged particles [2]. Agglomerates also obtain different SPSDs than spherical particles, depending on fractal dimension. The time it takes to reach the SPSD is about twice as long as the time it takes for a spherical particle:

3

Mathematical Models

The mathematical model of phase two of the nanoparticle production is based on the original Smoluchowski Equation (2.1). Logically, this involves a list of simplifications with respect to the actual physical properties and nanoparticle growth in the VSP-G1. The simplest model assumes pure spherical particle growth due coagulation in a closed space, neglecting aerosol transport and losses. It also claims that the physical properties can be defined in a constant molecular free regime.

A model in its earliest stage aims for mathematical and computational simplicity. This motivates the initial exclusion of agglomeration, the transport equation, secondary growth mechanisms, source or sink terms and changes due to a regime transition.

The basic model presented in this study (Section 3.1) obtains the particle size distribution $n(v)$, after a certain time t_R, which corresponds to the time particles have to coagulate during transport in the tube of the VSP-G1. A solution method which solves for $n(v)$ was obtained by Pafnuty Chebyshev in 1887. The Method of Moments (MoM) assumes particle volume conservation, an is therefore applicable for models approximating particle growth in a closed spaces (Section 3.2).

The MoM has been applied in a wide range of fields such as electromagnetism [17], planetary formation [18], finances, data processing [19], but also aerosol dynamics and nanotechnology [5, 6, 12, 20–23]. Frenklach and Harris used the MoM in 1987 to simulate nanoparticle growth mechanisms like nucleation, surface reaction and coagulation [23]. Without having to track the behavior of the entire PSD, the MoM extracts specific information of the coagulation process, so called "moments". The zeroth moment is equal to the total particle concentration $M_0(t) = N(t)$, the first moment resembles the constant total particle volume and the second moment is the total particle volume squared.

Having constructed a solvable, simple model for nanoparticle growth in the VSP-G1, possible expansions are stated in Section 3.3, and evaluated with respect to feasibility. Lastly, two other solution methods are introduced (Section 3.4), forming motivational groundwork for applying the Method of Moments in the current study.

3.1. COAGULATION IN A CLOSED SPACE WITHOUT AEROSOL TRANSPORT

The simplest computational model solves the original Smoluchowski Equation (2.1) and assumes coagulation occurs in an unchanged regime: free-molecular. It considers that coagulation takes place in a closed space, corresponding with the dimensions of the tube, over a fixed residence time t_R. The residence time is the total time that a particle spends inside the tube:

$$t_R = \frac{V_{tube}}{Q} = \frac{\pi d_{tube}^2 L}{4Q}, \tag{3.1}$$

where d_{tube} is the diameter of the tube; L is the length of the tube, Q is the carrier gas in ($m^3 s^{-1}$).

Recall (2.1),

$$\frac{\partial n(v,t)}{\partial t} = \frac{1}{2}\int_0^v \beta(v', v-v', t) n(v', t) n(v-v', t) dv' - n(v) \int_0^\infty \beta(v, v', t) n(v', t) dv',$$

where the transport equation is neglected, however transport of aerosol is incorporated in the model via a "detour". Let the total running time of the VSP-G1 be t_{TOTAL}, and $\tilde{N}$ be the total number of $t_R \in t_{\text{TOTAL}}$. First, the original Smoluchowski equation is solved for $0 < t < t_R$. The result is a PSD corresponding to a small fraction of the total particles, namely the particles that enter the tube at $t = 0$ and exit at $t = t_R$. This PSD is noted by $n(v)_{t_R}$. Once $n(v)_{t_R}$ is obtained, the final particle size distribution $n(v)_{t_{\text{TOTAL}}}$ is easily calculated with the assumption that $n(v)_{t_{R_1}} = n(v)_{t_{R_2}} = \ldots = n(v)_{t_{R_{\tilde{N}}}}$:

$$n(v)_{t_{\text{TOTAL}}} = n(v)_{t_R} \cdot \tilde{N} \tag{3.2}$$

The model is visualized below:

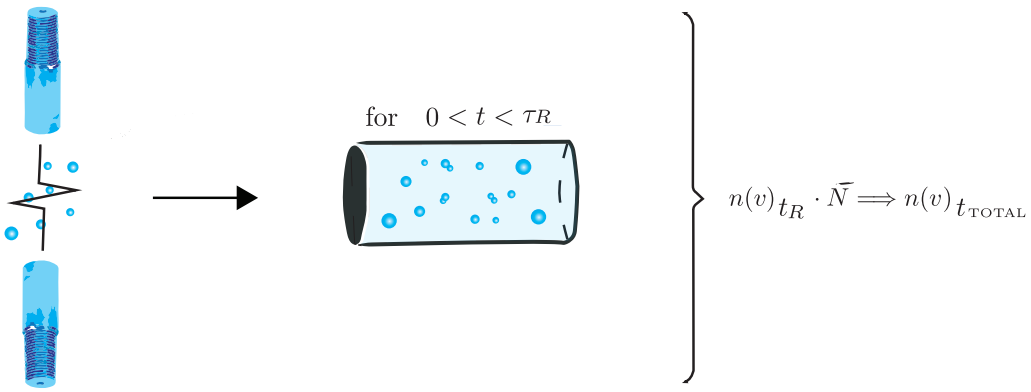

Figure 3.1: A computational model of coagulation in a closed space without aerosol transport

3.2. SOLUTION METHOD

A solution for the particle size distribution for a certain residence time $n(v)_{t_R}$ is obtained by solving the original Smoluchowski equation using the method of moments. The first task of the MoM is to convert the original Smoluchowski equation into a linearized momentum equation based on the size distribution [12]: the moment governing equation (Section 3.2.1). A specific variant: the log-normal method of moments (log-MoM) uses the assumption that the moment governing equation is a log-normal function. By doing so, a set of ordinary differential equations is given in Section 3.2.2. The result is a solution for the PSD of particles undergoing coagulation in the free-molecular regime.

3.2.1. MOMENT GOVERNING EQUATION

The derivation of the moment governing equation of the present study is followed according to [18]. Equation 2.1 can be written in terms of $n(v)$:

$$\frac{dn(v)}{dt} = \frac{1}{2}\int_0^v \beta(v', v-v')n(v')n(v-v')dv' - n(v)\int_0^\infty \beta(v,v')n(v')dv' \tag{3.3}$$

The k-th moment of the distribution, M^k, where k need not be an integer is defined as:

$$M_k = \int_0^\infty v^k n(v)dv \tag{3.4}$$

After five derivation steps (Appendix 6.1) the moment governing equation is obtained:

$$\frac{dM_k}{dt} = \frac{1}{2}\int_0^\infty \int_0^\infty \left[(v+v')^k - v^k - v'^k\right]\beta(v,v')n(v)n(v')dvdv' \tag{3.5}$$

Now the key is to convert the integral term on the RHS of (3.5) to a set of closed ordinary differential equations which represent the zeroth-, first- and second moment. Note, writing Equation 3.3 and 3.4 in terms of $n(v,t)$ will obtain the same set of ODE's.

3.2.2. LOG-NORMAL MOM

The log-normal method of moments (log-MoM) was developed by Cohen and Vaughan and assumes that the k^{th} moment is a function of time t, particle size v, mean particle size $v_g(t)$, and the geometric standard deviation based on particle radius $\sigma(t)$ [6]:

$$M_k(v,t) = \frac{1}{3\sqrt{2\pi}\ln\sigma(t)}v^k \exp\left[\frac{-\ln^2 v/v_g(t)}{18\ln^2\sigma(t)}\right]\frac{dv}{v} \tag{3.6}$$

Taking $k=0$ generates the particle size distribution as a function of time and volume [5], which is of most interest in the present study:

$$n(v,t) = \frac{1}{3v}\frac{N(t)}{\sqrt{2\pi}\ln\sigma(t)}\exp\left[\frac{-\ln^2 v/v_g(t)}{18\ln^2\sigma(t)}\right], \tag{3.7}$$

where $N(t) = M_0(t)$ is the total number concentration of particles. In order to solve this equation, expressions for $M_0(t), \sigma(t)$ and $v_g(t)$ are necessary [12, 18]:

$$v_g(t) = \frac{M_1^2}{M_0(t)^{3/2}M_2(t)^{1/2}} \tag{3.8}$$

$$\ln^2\sigma(t) = \frac{1}{9}\ln\left[\frac{M_0(t)M_2(t)}{M_1^2}\right] \tag{3.9}$$

From equation 3.5, the following set of ODEs is derived (Appendix 6.2 gives the complete derivation):

$$\begin{cases} \frac{dM_0}{dt} & = -bK_F(\frac{3}{4\pi})^{1/6}\left(M_0^{151/72}M_1^{-13/36}M_2^{19/72} + 2M_0^{131/72}M_1^{7/36}M_2^{-1/72} + M_0^{127/72}M_1^{11/36}M_2^{-5/72}\right) \\ \frac{dM_1}{dt} & = 0 \\ \frac{dM_2}{dt} & = 2bK_F(\frac{3}{4\pi})^{1/6}\left(M_0^{19/72}M_1^{-97/36}M_2^{31/72} + 2M_0^{-1/72}M_1^{-77/36}M_2^{11/72} + M_0^{-5/72}M_1^{-73/36}M_2^{7/72}\right) \end{cases} \tag{3.10}$$

Acceptable initial- and boundary conditions, along with a numerical descritezation method are used to solve the equations in 3.10 for M_0, M_1, M_2. Next, $v_g(t)$ and $\sigma(t)$ are computed with Equations 3.8 and 3.9, making it possible to obtain the particle size distribution with respect to time and particle volume from equation 3.7.

3.3. MODEL EXPANSIONS

A sufficient level of accuracy and model reliability is obtained by expanding the mathematical model with certain particle growth mechanisms or other physical phenomena.

An important element to incorporate in the current model is the effects of the a change in regime. Once the particle diameter exceeds a value of five nanometers, the collision frequency kernel will gradually shift from free-molecular to transition [14]. The geometric standard deviation of the PSD, σ, is characterized by its asymptotic behaviour, regardless of the regime an aerosol originates from [5]. It is necessary to test the current model on the same theoretical behaviour for both regimes.

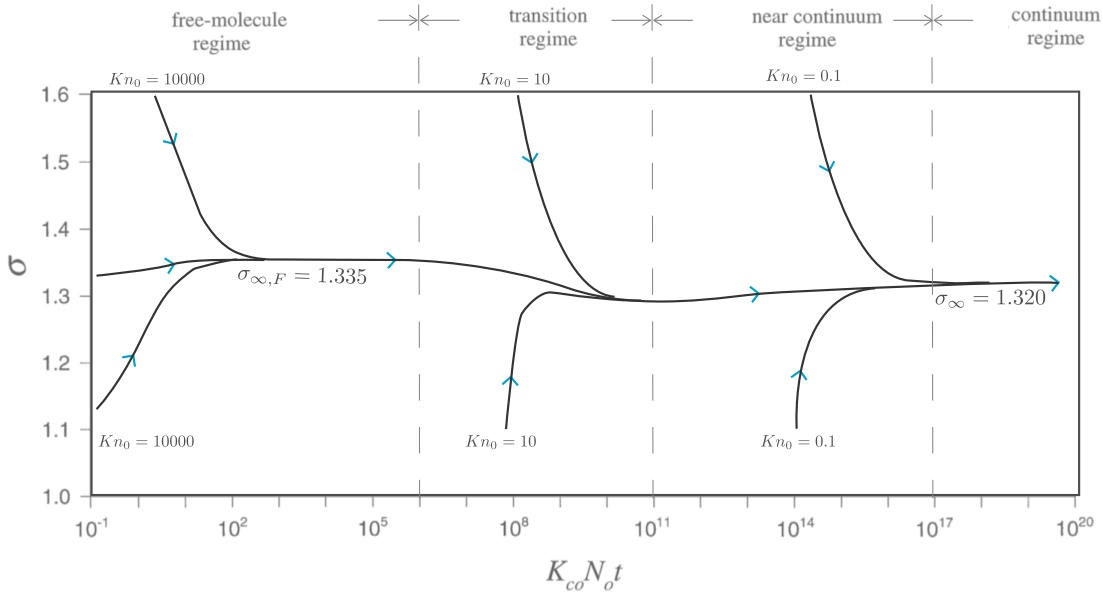

Figure 3.2: Change in the geometric standard deviation σ as a function of time as the particle size makes a transition from the free-molecule regime to the continuum regime. [5]

The logical next step is take agglomeration into account. Hypothetically, the corresponding computational aspects are comparable to that of the previous element, by simply incorporating a new type of collision kernel. However, further research is necessary with respect to interpretation and validation of the model results. It might be useful to look into how the fractal dimension can be added to the output, in order to classify the level of agglomeration. Validation with VSP-G1 measurements occurs with a Differential Mobility Analyzer (DMA), which measures the sizes of all electrically charged nanoparticles (± 10 % of the total produced nanoparticle concentration). Information on the DMA's ability to detect and classify agglomerates is needed for experimental validation of the extended model.

According to previous research conducted with the DMA, the total mass of a certain measured particle concentration, scaled to include both neutral and electrically charged particles, does not correspond with the total mass loss of the electrodes. This initiates aerosol loss, probably due to particle deposition in the spark chamber as well as on the tube wall. The corresponding loss of particles can be incorporated into the computational model with a simple sink term. [24] states that the particle loss due to turbulent diffusion to the wall and can be described as:

$$n_{\text{sink}}(v,t) = -4k(v)n(v,t)/d_{\text{tube}}, \tag{3.11}$$

where $k(v)$ is the size dependent mass transfer coefficient.

The assumption that the particle size distribution is equivalent for all residence times can also be challenged. If necessary, a stochastic factor can be applied to account for the effects of Brownian Motion.

Lastly, the effects of aerosol transport can be analyzed by incorporating the Navier Stokes Equation. Hypothetically, a new solution method is necessary to obtain the new PSD in terms of particle volume, time and space.

$$\frac{\partial n(v,x,t)}{\partial t} + \frac{\partial\big(un(v,x,t)\big)}{\partial x} = \\ -\frac{1}{2}\int_{v^*}^{v}\beta(v',v-v',t)n(v',x,t)n(v-v',t)dv' - n(v,t)\int_{v^*}^{\infty}\beta(v,v',t)n(v',x,t)dv' \tag{3.12}$$

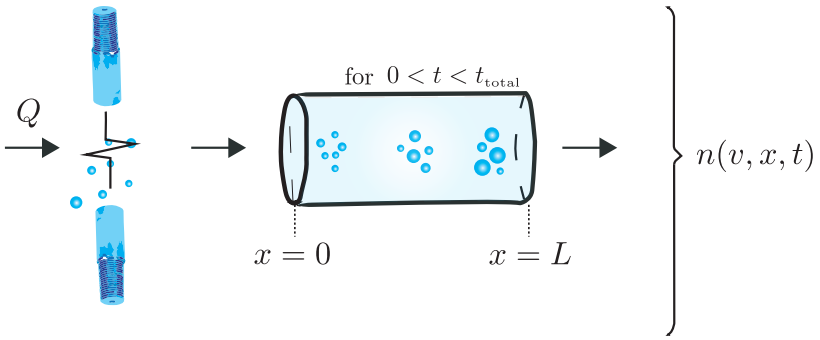

Figure 3.3: A computational model of coagulation in an open space with aerosol transport

3.4. OTHER SOLUTION METHODS

SECTIONAL METHOD

The sectional method solves the Smoluchowski Equation at every interval in terms of timestep, particle size and spacial location [18] and can therefore be applied to solve Equation 3.12. The solution is obtained using numerical discretization methods such as Runge Kutta to approximate the Smoluchowski integrals. A finite element scheme can be applied for the spacial coordinate of the transport equation [25]. The sectional method is used to study the evolution of the PSD over time [18], and generates the most detailed outcome. However, computational costs follow, making it quite impractical [12].

MONTE CARLO METHOD

A stochastic particles approach is the last alternative for computationally modelling the coagulation of nanoparticles. The method allows coagulation of two particles to occur with a certain probability and contains various algorithms; the direct simulation algorithm (DSA) and the mass flow algorithm (MFA) are the most popular. [26], [27]. The stochastic particles approach or, *Monte Carlo method*, allows the PSD to fully be determined along with the moments of the distribution. Also, it has proven to be computationally less expensive compared to the sectional method [27]. A draw back is that the derivation of a stochastic coagulation model is mathematically complex and requires a thorough understanding of probability theory. Moreover, the incorporation of computational fluid dynamics (CFD) is still limited [12].

The computational expense of the sectional method, and the complexity and limits of Monte Carlo are nonexistent in the Method of Moments. Although the original MoM is unable to trace the evolution of the particle size distribution, the log-normal MoM overcomes this by reconstructing the PSD from a log-normal distribution.

4

Implementation and Results

The model corresponding with coagulation in a closed space without aerosol transport, for the free - molecular regime is implemented. The initial conditions derived in Section 4.1 hold for all MoM techniques, though only the log-normal technique is treated in the present study. Section 4.2 obtains a dimensionless expression for the stiff set of ordinary differential equations derived in the previous chapter (Equation set 3.10).

A Forward Euler discretization method is used to solve the dimensionless set of equations. To validate the model with literature in Section 4.3, the particle concentration N and geometric mean particle volume v_g are derived in dimensionless form in terms of their initial values N_0 and v_{g0}, and compared with results obtained by Lee et al. [6]. Furthermore, the geometric standard deviation is calculated with Equation 3.9 and tested on asymptotic behaviour. All values are plotted against dimensionless time, $N_0 v_{g0}^{1/6} \tilde{K}_F t$. The dimensionless, log-normal MoM-based particle size distribution is derived and compared with the theoretical self-preserving size distribution (SPSD) [6] [2].

Section 4.4 obtains results from the initial conditions based on standard VSP-G1 settings. A sensitivity analysis is performed on the input parameters to obtain an understanding of the model behaviour. Finally, the dimensionless PSD is plotted against actual measurements.

Throughout Sections 4.3 and 4.4, the model is tested on accuracy and reliability with respect to theory [6] and to a data set generated by the DMA. The non-asymptotic behaviour of the PSD indicates a possible implementation error. Furthermore, a better understanding of VSP-G1 measurement techniques is needed in order to validate the model with the actual nanoparticle production of the system.

4.1. Initial conditions

The properties of the log-normal function are such that the following equation holds for any kth moment [6]:

$$M_k = M_0 v_g^k \exp\left(\frac{9}{2} k^2 \ln^2(\sigma)\right), \tag{4.1}$$

Equation 4.1 is applied to retrieve the initial conditions:

$$M_0(0) = N_0 \tag{4.2}$$

$$M_1(0) = M_1(t) = N_0 v_{g0} \exp\left(\frac{9}{2} \ln^2(\sigma_0)\right) \tag{4.3}$$

$$M_2(0) = N_0 v_{g0}^2 \exp\left(18 \ln^2(\sigma_0)\right), \tag{4.4}$$

It is can be seen that the initial conditions fully depend on the initial values for the particle number concentration N_0, geometric mean particle volume v_{g0}, and the geometric standard deviation based on particle size σ_0.

N_0 is derived from a list of input variables: ablation power P_A (W), spark frequency f (s^{-1}), molecular mass m_m (kg/mol), Avogadro's number N_A (atoms/mol), and the residence time t_R (s). The computations leading to the derivation of N_0 are schematized in Figure 4.1, where input variables that are controllable by the VSP-G1 are colored grey.

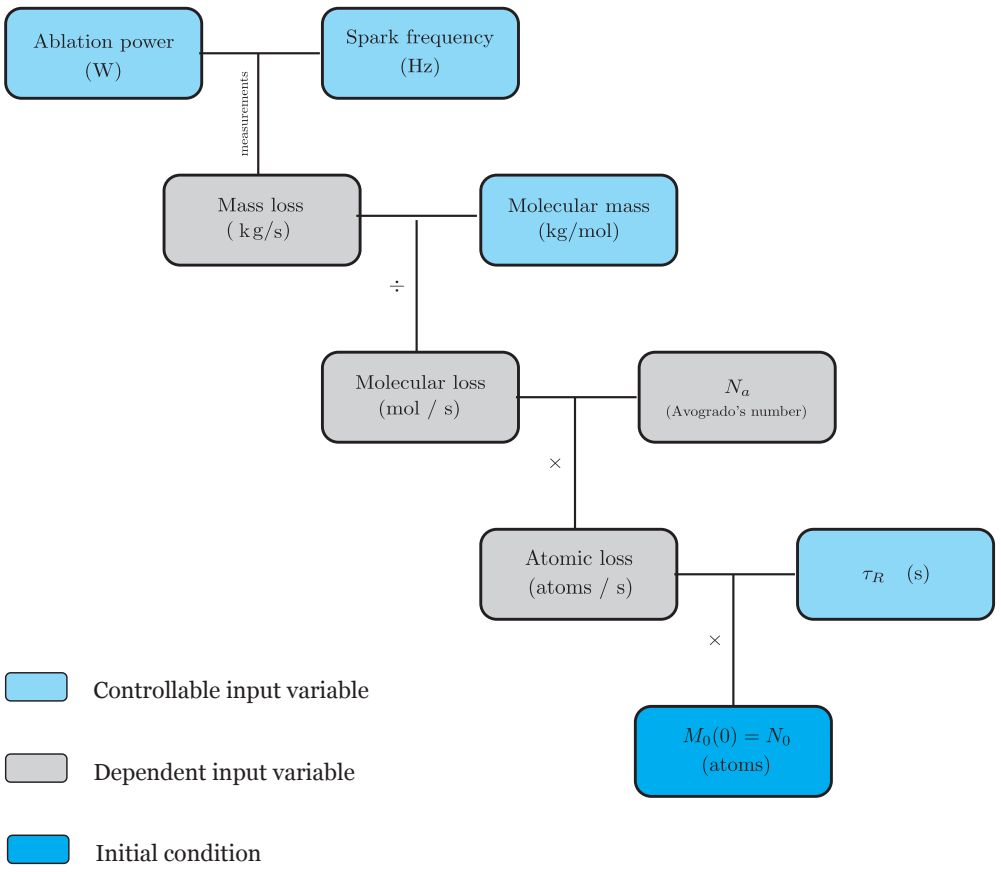

Figure 4.1: Derivation of initial particle concentration N_0

Furthermore, the initial geometric volume depends on the initial geometric particle radius:

$$v_{g0} = \frac{4r_{g0}^3}{3\pi}$$

A value for the initial geometric spread with respect to particle size σ_0 is based on either previous literature or measurements.

INITIAL CONDITIONS CORRESPONDING TO MONOTONE INITIAL AEROSOL

Under the assumption that spark ablation provides a monotone aerosol consisting of single atoms of pure material, the following initial conditions hold:

$$\begin{aligned} v_{g0} &= \frac{4r_p^3}{3\pi} \\ \sigma_0 &= 1 \\ M_0(0) &= N_0 \\ M_1(0) &= M_1(t) = N_0 v_{g0} \\ M_2(0) &= N_0 v_{g0}^2 \end{aligned}$$

4.2. NONDIMENSIONALIZATION

Given the system of ODE's from 3.10, for $0 < t < t_R$:

$$\begin{cases} \frac{dM_0}{dt} &= -bK_F(\frac{3}{4\pi})^{1/6}\left(M_0^{151/72}M_1^{-13/36}M_2^{19/72} + 2M_0^{131/72}M_1^{7/36}M_2^{-1/72} + M_0^{127/72}M_1^{11/36}M_2^{-5/72}\right) \\ \frac{dM_2}{dt} &= 2bK_F(\frac{3}{4\pi})^{1/6}\left(M_0^{19/72}M_1^{-97/36}M_2^{31/72} + 2M_0^{-1/72}M_1^{-77/36}M_2^{11/72} + M_0^{-5/72}M_1^{-73/36}M_2^{7/72}\right) \end{cases} \tag{4.5}$$

The unscaled set of equations is extremely stiff which results in numerical instability. Using an extremely small step size isn't suitable and therefore nondimensionalizing the set of ODE's is necessary. The following dimensionless parameters for t, M_0 and M_2 have been introduced by previous research [6], [5], [14]:

$$\tau = \nu_{g0}^{1/6}\tilde{K}_F N_0 t \tag{4.6}$$

$$\widetilde{M_0} = M_0 M_0(0)^{-1} \tag{4.7}$$

$$\widetilde{M_2} = M_2 M_2(0)^{-1} \tag{4.8}$$

Also, let $b(t) = b(\tau(\nu_{g0}^{1/6}\tilde{K}_F N_0)^{-1}) = B(\tau)$.

Expressing 4.5 in terms of the previously defined dimensionless parameters obtains the following dimensionless ordinary differential problem (the complete derivation is given in Appendix 6.3).

Given the dimensionless set of ordinary differential equations for $0 < \tau < \tau_R$:

$$\begin{cases} \frac{d\widetilde{M_0}}{d\tau} &= -B(\tau)\left(\widetilde{M_0}^{151/72}\widetilde{M_2}^{19/72} + 2\widetilde{M_0}^{131/72}\widetilde{M_2}^{-1/72} + \widetilde{M_0}^{127/72}\widetilde{M_2}^{-5/72}\right) \\ \frac{d\widetilde{M_2}}{d\tau} &= 2B(\tau)\left(\widetilde{M_0}^{19/72}\widetilde{M_2}^{31/72} + 2\widetilde{M_0}^{-1/72}\widetilde{M_2}^{11/72} + \widetilde{M_0}^{-5/72}\widetilde{M_2}^{7/72}\right) \end{cases} \tag{4.9}$$

with initial conditions:

$$\begin{cases} \widetilde{M_0}(0) = 1 \\ \widetilde{M_2}(0) = 1 \end{cases} \tag{4.10}$$

4.3. RESULTS WITH RESPECT TO THEORY

Solving System 4.9 allows the accuracy of the model to be tested with respect to results obtained by literature research by Lee et al. [6] (Figure 4.2).

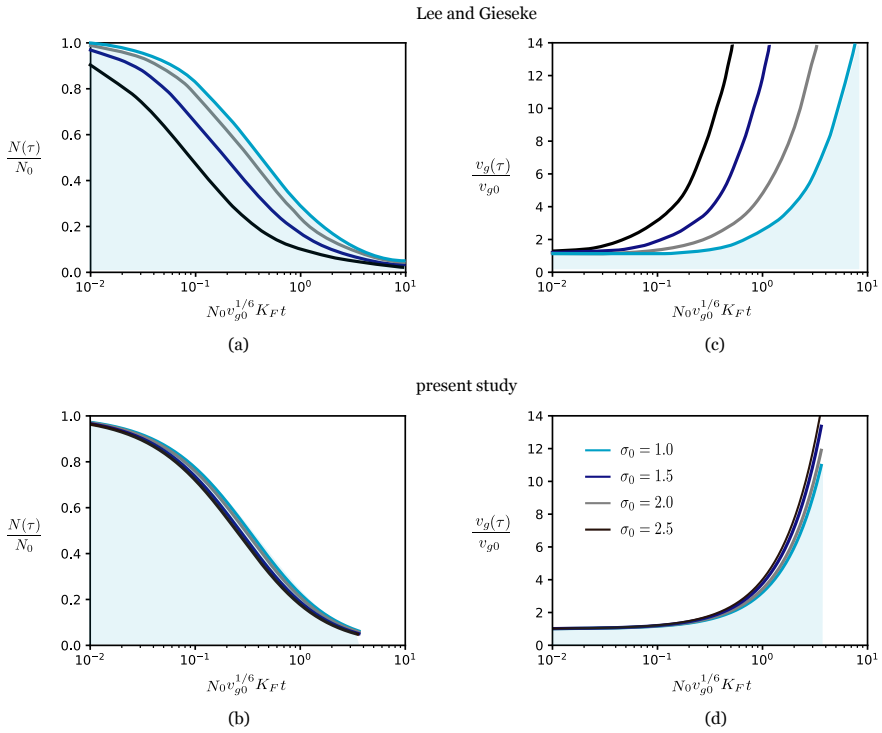

Figure 4.2: (a) Lee's dimensionless particle concentration. (b) present study's dimensionless particle concentration. (c) Lee's dimensionless particle volume. (d) present study's dimensionless particle volume. All functions are dependent on dimensionless time $\tau = N_0 v_{g0}^{1/6} K_F t$

Differences between Lee's results and the values obtained from this present study are mainly visible in Figure 4.3, which shows a different course of the geometric standard deviation with respect to dimensionless time. Lee et al. (top plot) claims that the dimensionless size distribution experiences asymptotic behaviour and approaches a fixed geometric standard deviation, $\sigma_\infty = 1.355$, independently of the initial size spread of the distribution σ_0 [6]. The same behavious is observed by Kodas [2] and Park [14] (recall Figure 3.2 in Section 3.3).

The present model assumes a monodisperse initial size distribution ($\sigma_0 = 1$). Although the corresponding geometric spread does approach the equivalent limit as Lee et al., the course of the other functions for σ deny any asymptotic behaviour of the PSD.

This may indicate an error in the implementation of the log-normal method of moments in the present study, possibly due to the assumption that coagulation occurs in a constant free-molecular regime, neglecting increase in polydispersity of the aerosol.

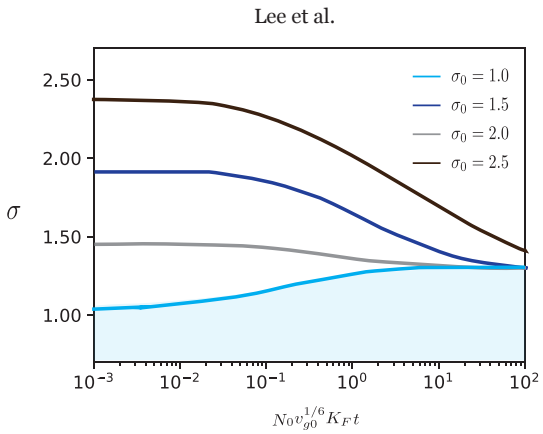

(a)

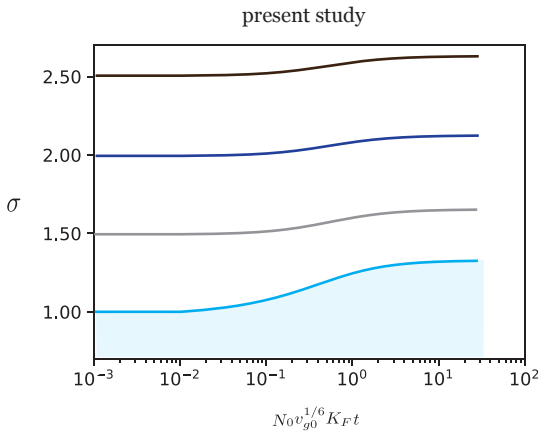

(b)

Figure 4.3: Geometric spread of particle size derived by to Lee. et al [6] (a). The geometric spread of particle size obtained in the present study (b)

DIMENSIONLESS PARTICLE SIZE DISTRIBUTION

Recall the self-preserving size distribution $\varphi(v/v_g)$ in Equation 2.17. An equivalent, time-dependent form of the distribution function is achieved when writing the expression for the PSD defined in Equation 3.7 in dimensionless form in terms of $N/N(\tau)$ and $v/v_g(\tau)$,

$$\frac{n(v,\tau)v}{N(\tau)} = \frac{1}{3\sqrt{2\pi}\ln\sigma(\tau)} \exp\left[\frac{-\ln^2\left(v/v_g(\tau)\right)}{18\ln^2\left(\sigma(\tau)\right)}\right], \tag{4.11}$$

Figure 4.4 shows a comparison of Function 4.11 for various residence times $\tau = \{\tau_R, 2\tau_R, 4\tau_R\}$, with a self-preserving size distribution obtaining a constant spread $\sigma_\infty = 1.335$. In theory, $\frac{n(v,\tau_R)v}{N(\tau)}$ will approach $\varphi(\eta)$. However for $\sigma_0 \neq 1.0$, results don't comply due to the previously observed non-asymptotic behaviour of σ (Figure 4.3).

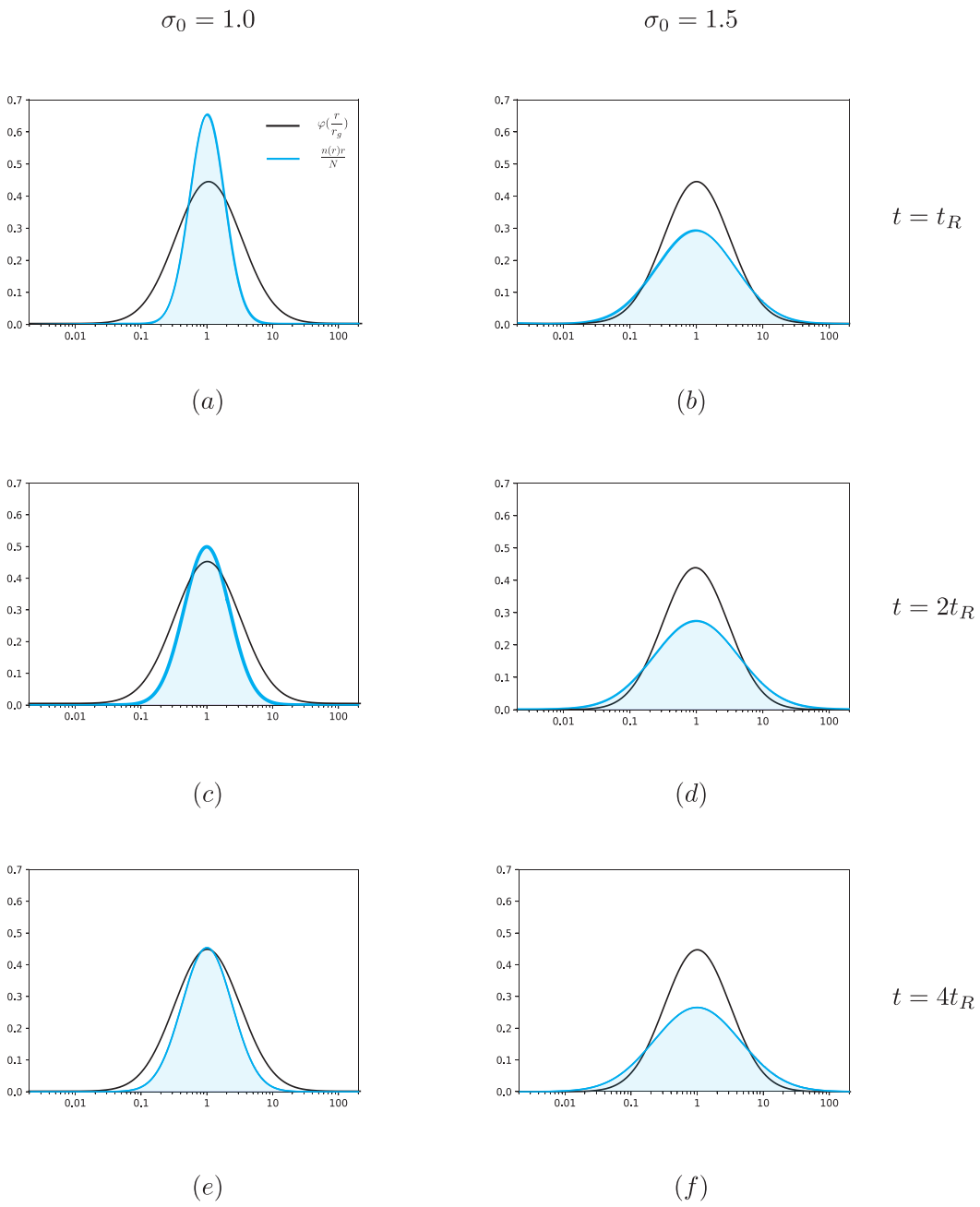

Figure 4.4: The dimensionless PSD in terms of particle volume, $\frac{n(v)v}{N}$ (Equation 4.11) and the self-preserving particle size distribution in terms of particle radius $\varphi(v)$ with $\sigma_\infty = 1.355$ (Equation 2.17). Results are plotted for two different initial geometric size standard deviations $\sigma_0 = 1.0$ (left) and $\sigma_0 = 1.5$ (right), and for three different residence times with $t_R = 0.42$s. The y-axis is defined by $\frac{n(v)v}{N}$, the x-axis is defined by $\frac{v}{v_g}$.

4.4. RESULTS WITH RESPECT TO VSP-G1

The following results are obtained with inputs that correspond to conditions applicable for the VSP-G1. The ablated material is gold, with a particle radius of 135 pm. The settings of the G1 correspond with 1 L/min inflow ,5 J/s ablation power, 175 Hz spark frequency, 1 m tube length, 3 mm tube diameter and a temperature of 296.15 K. These conditions result in the following initial values and residence time:

$$
\begin{aligned}
N_0 &= 4 \times 10^{14}\,\text{particles} \\
v_{g0} &= 1 \times 10^{-30}\,\text{m}^3 \\
\sigma_0 &= 1.0 \\
t_R &= 0.42\,\text{s}
\end{aligned}
$$

The relative particle concentration is generated by solving System 4.9 for the dimensionless zeroth- and second moment $\widetilde{M_0}\widetilde{M_2}$. The relative geometric mean particle volume and the geometric spread of particle size are generated by equations 3.8 and 3.9 respectively:

$$
\begin{aligned}
v_g(t) &= \frac{M_1^2}{M_0(t)^{3/2} M_2(t)^{1/2}} \\
\ln^2 \sigma(t) &= \frac{1}{9} \ln \left[\frac{M_0(t) M_2(t)}{M_1^2} \right]
\end{aligned}
$$

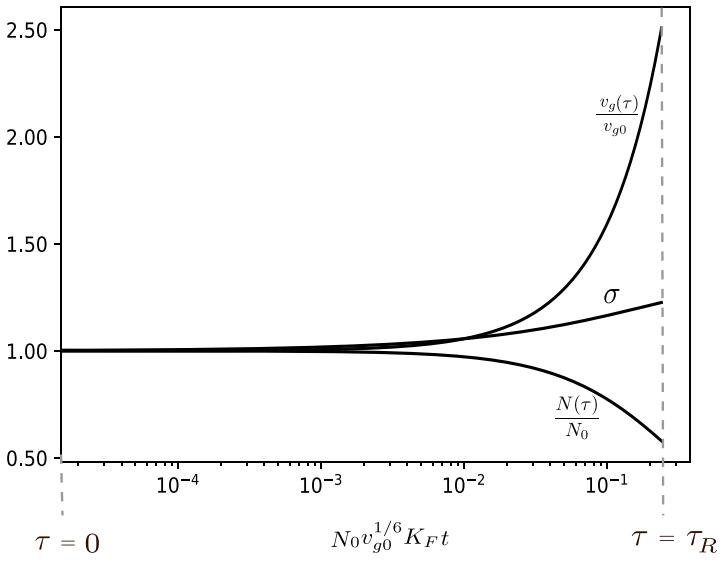

Figure 4.5: the relative particle concentration $\frac{N(\tau)}{N_0}$, the relative particle volume $\frac{v_g(\tau)}{v_{g0}}$ and the geometric spread of particle size σ as a function of dimensionless time τ for initial conditions corresponding to the VSP-G1 standard settings.

It is observed in Figure 4.5a that the total particle concentration decreases with about 45%, this corresponds to a geometric mean particle volume increase of 250%. The geometric standard deviation increases with 20%.

MODEL BEHAVIOUR

A parameter sensitive analysis is conducted to obtain an understanding of the computational model, focusing on the influence of initial conditions on the coagulation rate. Increasing the ablation power has a direct

positive influence on the initial concentration. Logically the particle concentration will experience a larger decrease, due to the fact that particles will encounter each other, collide and fuse more frequently when considering a constant space. This proposition also initiates an increase of mean particle volume after time t_R.

One might think that increasing the tube length will have the opposite effect, as the chance of inter-particle collision decreases. However, this effect is some what canceled out by the increase of residence time, recall the definition for t_R in Equation 3.1.

The initial particle volume, determined by the initial particle radius, also determines the rate of coagulation. However modifying v_{g0} is five time less effective on the final results than modifying N_0. Logically, this effect is clarified when one understands the physical aspects of the problem.

PARTICLE SIZE DISTRIBUTION

Figure 4.6 compares the PSD generated in this present study (blue), with actual VSP-G1 measurements (black). Equation 4.11 is defined in terms of the particle radius r, and plotted for residence times: $t_R = 190\,\text{ms}, 340\,\text{ms}$ and 490 ms. The data sets are generated by a differential mobility analyzer (DMA) to measure particle size concentration. The DMA excludes particles with no electric charge (90% of the aerosol), and particles exceeding a certain radius. The latter causes a mode shift to the right, as the particle radius is scaled to the mean particle radius of the corresponding data set.

The modes obtained by the computational model are comparable to the DMA measurement. However, measurements obtained from other data sets are not as consistent. Therefore a better understanding of the DMA measurement technique is required in order to analyze the accuracy of the model with respect to VSP-G1 measurements.

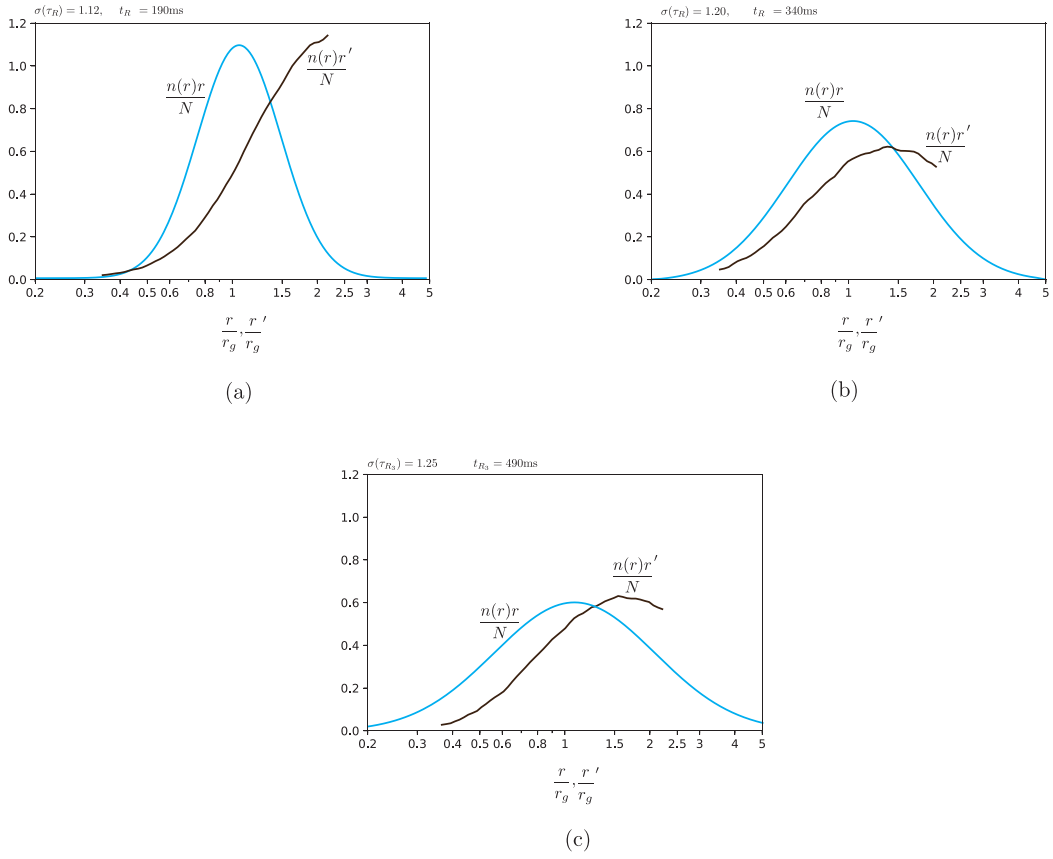

Figure 4.6: PSD from log-normal MoM based model (top), PSD from VSP-G1 data measurements (bottom). (a) for $\tau_R = 190ms$, (b) for $\tau_R = 340ms$, (c) for $\tau_R = 490ms$.

5

CONCLUSIONS

This literature study provides the theoretical background necessary to develop a complete, accurate and efficient computational model of nanoparticle growth in the VSP-G1. A first version of the model has been developed, assuming the most basic physical conditions: nanoparticle growth due to coagulation, in a closed space, for a constant (free molecular) regime. Subsequently, the results are tested with respect to previous research [6] and VSP-G1 measurements. Observed is that the resulting particle size distribution doesn't obtain the required asymptotic behaviour. This could be the result of a computational error. Another hypothesis is that excluding the computational aspects of the transition regime prohibits the model to take the effects of an increasing polydispersity into account.

Furthermore, this literature study prospects on the possibilities to expand the model, which will eventually provide a model for nanoparticle growth in the VSP-G1 consisting of sufficient accuracy, efficiency and reliability. Corresponding research questions, goals and approach are stated in this chapter prospecting on the remaining part of this thesis.

5.1. PRELIMINARY RESEARCH QUESTIONS

"How can nanoparticle growth in the VSP-G1 be modelled to study the particle size distribution?"

In the course of this thesis, the aim is to address the main research question stated above. The corresponding sub-questions are:

1. What is causing the non-asymptotic behaviour of the particle size distribution in the current version of the model?
2. What is the effect of incorporating the transition regime on the accuracy of the output?
3. Consider the following possible elements for model expansion: agglomeration, sink/source term, transport equation and other growth mechanisms. Which elements are most feasible to implement?
4. When incorporating agglomeration, how can the results be interpreted with respect to particle size and shape?
5. How sensitive is the model to perturbations of the input parameters. Can the accuracy of the input parameters be improved?
6. What is the quality of the numerical model and can it be improved?
7. How does the final model perform compared to measurements provided by VSPARTICLE?

5.2. GOALS & METHODOLOGY

"Develop an accurate and computationally efficient numerical model which describes the growth of nanoparticles produced in the VSP-G1."

The main goal is reached by the approach below. Completing all steps, each coupled to a previously stated research question, will eventually result in obtaining a sufficient computational model for the nanoparticle growth in the VSP-G1.

1. Obtain a grounded explanation for the non-asymptotic behaviour of the PSD. The computational model will be thoroughly reviewed for implementation errors, with respect to the model developed by Lee [6]. Alternatively, look into the effect of incorporating the transition regime.

2. Introduce the physical aspects of nanoparticles entering the transition regime by gradually incorporating the transition collision frequency kernel β_T.

3. Conduct a feasibility analysis on model expansion possibilities with respect to computational and mathematical complexity and their predicted impact on model accuracy. Incorporate the most feasible element(s).

4. Incorporate agglomeration into the model by adding the corresponding collision frequency kernel. Conduct research on the interpretation and classification of agglomerates in a particle size distribution, and the ability to measure agglomeration for instance with the DMA. Finally, the results will be analyzed respect to agglomeration.

5. Once the model obtains a sufficient level of accuracy and efficiency, a sensitivity analysis with respect to the controllable input parameters will be performed.

6. Perform a numerical analysis, testing the model on stability, order and convergence.

7. Compare the results obtained from the model with measurements from the VSP-G1. Conclude on the accuracy, efficiency and reliability of the model.

6

APPENDIX

6.1. MOMENT GOVERNING EQUATION

Given the Smoluchowski equation expressed in terms of $n(v)$:

$$\frac{dn(v)}{dt} = \frac{1}{2}\int_0^v \beta(v', v-v')n(v')n(v-v')dv' - n(v)\int_0^\infty \beta(v,v')n(v')dv' \tag{6.1}$$

The k-th moment of the distribution, M^k, where k need not be an integer is defined as:

$$M_k = \int_0^\infty v^k n(v)dv \tag{6.2}$$

Step A

Both sides of the equation 6.1 is multiplied by v^k and both sides are integrated over volume v. Also, (6.2) is inserted on the RHS.

$$\frac{dM_k}{dt} = \int_0^\infty v^k \frac{dn}{dt}dv = \frac{1}{2}\int_0^\infty\int_0^v v^k\beta(v', v-v')n(v-v')n(v')dv'dv - \int_0^\infty\int_0^\infty v^k\beta(v,v')n(v)n(v')dv'dv \tag{6.3}$$

Step B

A Heaviside function, $H(v-v')$, is introduced such that:

$$H(v-v') = \begin{cases} 1 & v-v' \geq 0 \\ 0 & v-v' < 0 \end{cases}$$

to extend the limits of the integral over v' from $(0, v)$ to $(0, \infty)$.

$$\frac{dM_k}{dt} = \frac{1}{2}\int_0^\infty\int_0^v v^k H(v-v')\beta(v', v-v')n(v-v')n(v')dv'dv - \int_0^\infty\int_0^\infty v^k\beta(v,v')n(v)n(v')dv'dv \tag{6.4}$$

Step C

The substitution $u = v - v'$, $du = dv$ and $v^k = (u+v')^k$ in equation 6.4. As the first integral is integrated over purely positive values for u, the Heaviside function is always equal to one.

$$\frac{dM_k}{dt} = \frac{1}{2}\int_0^\infty\int_0^\infty (u+v')^k\beta(u,v')n(u)n(v')dv'du - \int_0^\infty\int_0^\infty v^k\beta(v,v')n(v)n(v')dv'dv \tag{6.5}$$

Step D

Without loss of generality, the subsitution v for u is allowed and both integrals can be taken in one. The result is the moment equation:

$$\frac{dM_k}{dt} = \int_0^\infty \int_0^\infty \left[\frac{1}{2}(v+v')^k - v^k\right]\beta(v,v')n(v)n(v')dvdv' \tag{6.6}$$

Step E
Due to symmetry the equation above also holds for $v^k = v'^k$, which means the moment equation can be rewritten:

$$\frac{dM_k}{dt} = \frac{1}{2}\int_0^\infty \int_0^\infty \left[(v+v')^k - v^k - v'^k\right]\beta(v,v')n(v)n(v')dvdv' \tag{6.7}$$

6.2. DERIVATION OF ODES USING LOG-NORMAL MOM

Given equation 6.7, it is observed that the collision frequency kernel β is present in the moment governing equation. Due to the assumption that particle growth occurs in a constant regime, a set of ODE's is derived using the log-normal MoM for the free molecular regime.

In the free-molecular regime, it is difficult to expand the kernel β_F (equation 2.6) into a power series [28]. Therefore, a coefficient b is introduced such that: $\sqrt{\frac{1}{v_i}+\frac{1}{v_j}} = b\left(\sqrt{\frac{1}{v_i}}+\sqrt{\frac{1}{v_j}}\right)$. The coefficient b is dependent on the polydisperisty of the aerosol [5], which is represented by the geometric spread of the particle size distribution σ. The function b is fitted to only depend on σ by Park, Lee, Otto and Fissan in [5]:

$$b = 1 + 1.2\exp(-2\sigma) - 0.646\exp(-0.35\sigma^2) \tag{6.8}$$

The collision frequency kernel for the free-molecular regime is rewritten in the following form:

$$\beta_F(v_i,v_j) = bK_F(\frac{3}{4\pi})^{1/6}\left(\sqrt{\frac{1}{v_i}}+\sqrt{\frac{1}{v_j}}\right)\left(v_i^{1/3}+v_j^{1/3}\right)^2 \tag{6.9}$$

Inserting the new expression for β_F into the moment governing equation gives:

$$\begin{aligned}\frac{dM_k}{dt} &= \frac{bK_F}{2}(\frac{3}{4\pi})^{1/6}\int_0^\infty\int_0^\infty\left[(v+v')^k - v^k - v'^k\right]\left(\sqrt{\frac{1}{v_i}}+\sqrt{\frac{1}{v_j}}\right)\left(v_i^{1/3}+v_j^{1/3}\right)^2 n(v)n(v')dvdv' \\ &= \frac{bK_F}{2}(\frac{3}{4\pi})^{1/6}\int_0^\infty\int_0^\infty\left[(v+v')^k - v^k - v'^k\right]\left(v^{1/6}v'^{1/6}\frac{2v^{1/3}}{v'^{1/6}}+\frac{2v'^{1/3}}{v^{1/6}}+\frac{v'^{2/3}}{v^{1/2}}+\frac{v^{2/3}}{v'^{1/2}}\right)n(v)n(v')dvdv'\end{aligned} \tag{6.10}$$

Let $k=0$, $k=1$ and $k=2$:

$$\begin{cases}\frac{dM_0}{dt} &= -\frac{bK_F}{2}(\frac{3}{4\pi})^{1/6}\int_0^\infty\int_0^\infty\left(v^{1/6}v'^{1/6}\frac{2v^{1/3}}{v'^{1/6}}+\frac{2v'^{1/3}}{v^{1/6}}+\frac{v'^{2/3}}{v^{1/2}}+\frac{v^{2/3}}{v'^{1/2}}\right)n(v)n(v')dvdv' \\ \frac{dM_1}{dt} &= 0 \\ \frac{dM_2}{dt} &= \frac{bK_F}{2}(\frac{3}{4\pi})^{1/6}\int_0^\infty\int_0^\infty(2vv')\left(v^{1/6}v'^{1/6}\frac{2v^{1/3}}{v'^{1/6}}+\frac{2v'^{1/3}}{v^{1/6}}+\frac{v'^{2/3}}{v^{1/2}}+\frac{v^{2/3}}{v'^{1/2}}\right)n(v)n(v')dvdv'\end{cases} \tag{6.11}$$

Then, relation (6.2) is used to transform the RHS of (6.11) as a function of fractal moments:

$$\begin{cases}\frac{dM_0}{dt} &= -bK_F(\frac{3}{4\pi})^{1/6}\left(M_{1/6}M_0 + 2M_{1/3}M_{-1/6} + M_{2/3}M_{-1/2}\right) \\ \frac{dM_1}{dt} &= 0 \\ \frac{dM_2}{dt} &= 2bK_F(\frac{3}{4\pi})^{1/6}\left(M_{7/6}M_1 + 2M_{4/3}M_{5/6} + M_{1/2}M_{5/3}\right)\end{cases} \tag{6.12}$$

In order to close the set of ODEs in (6.12) the property of a log-normal function ensuring that any k^{th}, where k not need be an integer, may be expressed as:

$$M_k = M_0 v_g^k \exp\left(\frac{9}{2} k^2 \ln^2(\sigma)\right), \tag{6.13}$$

is used. Rewriting (6.13) in terms of v_g and σ for $k = 0, k = 1, k = 2$ gives:

$$v_g = \frac{M_1^2}{M_0^{3/2} M_2^{1/2}} \tag{6.14}$$

$$\ln^2 \sigma = \frac{1}{9} \ln\left[\frac{M_0 M_2}{M_1^2}\right] \tag{6.15}$$

Inserting (6.13, 6.14, 6.15) into the set of unclosed moment governing equations (6.12) closes the set of ODE's and completes step 2:

$$\begin{cases} \frac{dM_0}{dt} &= -bK_F(\frac{3}{4\pi})^{1/6}\left(M_0^{151/72} M_1^{-13/36} M_2^{19/72} + 2M_0^{131/72} M_1^{7/36} M_2^{-1/72} + M_0^{127/72} M_1^{11/36} M_2^{-5/72}\right) \\ \frac{dM_1}{dt} &= 0 \\ \frac{dM_2}{dt} &= 2bK_F(\frac{3}{4\pi})^{1/6}\left(M_0^{19/72} M_1^{-97/36} M_2^{31/72} + 2M_0^{-1/72} M_1^{-77/36} M_2^{11/72} + M_0^{-5/72} M_1^{-73/36} M_2^{7/72}\right) \end{cases} \tag{6.16}$$

6.3. NONDIMENSIONALIZATION

Given the system of ODE's from for $0 < t < t_R$:

$$\begin{cases} \frac{dM_0}{dt} &= -bK_F(\frac{3}{4\pi})^{1/6}\left(M_0^{151/72} M_1^{-13/36} M_2^{19/72} + 2M_0^{131/72} M_1^{7/36} M_2^{-1/72} + M_0^{127/72} M_1^{11/36} M_2^{-5/72}\right) \\ \frac{dM_2}{dt} &= 2bK_F(\frac{3}{4\pi})^{1/6}\left(M_0^{19/72} M_1^{-97/36} M_2^{31/72} + 2M_0^{-1/72} M_1^{-77/36} M_2^{11/72} + M_0^{-5/72} M_1^{-73/36} M_2^{7/72}\right) \end{cases} \tag{6.17}$$

To generate a dimensionless system of equations, each variable is replaced by a quantity scaled relative to a characteristic unit of measure, noted by the subscript c, which are yet to be determined.

Set $M_0 = \widetilde{M}_0 M_{0c}$, $M_2 = \widetilde{M}_2 M_{2c}$ and $t = \tau t_c$. Also, let $b(t) = b(\tau t_c) = B(\tau)$ and fill the these new definitions into set of equations 6.17.

$$\begin{aligned} \frac{d\widetilde{M}_0}{d\tau}\frac{M_{0c}}{t_c} &= -B(\tau)K_F(\frac{3}{4\pi})^{1/6}\Big((\widetilde{M}_0 M_{0c})^{151/72} M_1^{-13/36} (\widetilde{M}_2 M_{2c})^{19/72} + \dots \\ &\quad \dots 2(\widetilde{M}_0 M_{0c})^{131/72} M_1^{7/36} (\widetilde{M}_2 M_{2c})^{-1/72} + (\widetilde{M}_0 M_{0c})^{127/72} M_1^{11/36} (\widetilde{M}_2 M_{2c})^{-5/72}\Big) \\ \frac{d\widetilde{M}_2}{d\tau}\frac{M_{2c}}{t_c} &= 2B(\tau)K_F(\frac{3}{4\pi})^{1/6}\Big((\widetilde{M}_0 M_{0c})^{19/72} M_1^{-97/36} (\widetilde{M}_2 M_{2c})^{31/72} + \dots \\ &\quad \dots 2(\widetilde{M}_0 M_{0c})^{-1/72} M_1^{-77/36} (\widetilde{M}_2 M_{2c})^{11/72} + (\widetilde{M}_0 M_{0c})^{-5/72} M_1^{-73/36} (\widetilde{M}_2 M_{2c})^{7/72}\Big) \end{aligned}$$

For simplicity, introduce $f(M_0, M_2)$ and $g(M_0, M_2)$, and $\tilde{K}_F = K_F(\frac{3}{4\pi})^{1/6}$, .

$$\begin{aligned} \frac{d\widetilde{M}_0}{d\tau}\frac{M_{0c}}{t_c} &= -B(\tau)\tilde{K}_F f\Big(\widetilde{M}_0 M_{0c}, \widetilde{M}_2 M_{2c}\Big) \\ \frac{d\widetilde{M}_2}{d\tau}\frac{M_{2c}}{t_c} &= 2B(\tau)\tilde{K}_F g\Big(\widetilde{M}_0 M_{0c}, \widetilde{M}_2 M_{2c}\Big) \end{aligned}$$

Divide by $\frac{M_{0c}}{t_c}$ and $\frac{M_{2c}}{t_c}$

$$\begin{aligned} \frac{d\widetilde{M}_0}{d\tau} &= -B(\tau)\frac{t_c}{M_{0c}}\tilde{K}_F f\Big(\widetilde{M}_0 M_{0c}, \widetilde{M}_2 M_{2c}\Big) \\ \frac{d\widetilde{M}_2}{d\tau} &= 2B(\tau)\frac{t_c}{M_{2c}}\tilde{K}_F g\Big(\widetilde{M}_0 M_{0c}, \widetilde{M}_2 M_{2c}\Big) \end{aligned}$$

The characteristic units of measure t_c, M_{0c} and M_{2c} are defined next. A wide range of literature [6], [5], [14], take the dimensionless time as

$$\tau = v_{g0}^{1/6} \tilde{K}_F N_0 t,$$

which leads to $t_c = \left(v_{g0}^{1/6} \tilde{K}_F N_0\right)^{-1}$. A logic choice for the remaining units of measure is: $M_{0c} = N_0$ and $M_{2c} = N_0 v_g(0)^2$. After some rearranging the dimensionless set of ODE's is obtained:

$$\begin{cases} \frac{d\widetilde{M_0}}{d\tau} &= \frac{-B(\tau)}{v_{g0}^{1/6} N_0^2} f\left(\widetilde{M_0} N_0, \widetilde{M_2} N_0 v_{g0}^2\right) \\ \frac{d\widetilde{M_2}}{d\tau} &= \frac{2B(\tau)}{v_{g0)}^{11/6} N_0^2} g\left(\widetilde{M_0} N_0, \widetilde{M_2} N_0 v_{g0}^2\right) \end{cases}$$

$$\begin{cases} \frac{d\widetilde{M_0}}{d\tau} &= \frac{-B(\tau)}{v_{g0}^{1/6} N_0^2} \Big((\widetilde{M_0} N_0)^{151/72} (N_0 v_{g0})^{-13/36} (\widetilde{M_2} N_0 v_{g0}^2)^{19/72} + \dots \\ & \dots 2(\widetilde{M_0} N_0)^{131/72} (N_0 v_{g0})^{7/36} (\widetilde{M_2} N_0 v_{g0}^2)^{-1/72} + (\widetilde{M_0} N_0)^{127/72} (N_0 v_{g0})^{11/36} (\widetilde{M_2} N_0 v_{g0}^2)^{-5/72} \Big) \\ \frac{d\widetilde{M_2}}{d\tau} &= \frac{2B(\tau)}{v_{g0)}^{11/6} N_0^2} \Big((\widetilde{M_0} N_0)^{19/72} (N_0 v_{g0})^{-97/36} (\widetilde{M_2} N_0 v_{g0}^2)^{31/72} + \dots \\ & \dots 2(\widetilde{M_0} N_0)^{-1/72} (N_0 v_{g0})^{-77/36} (\widetilde{M_2} N_0 v_{g0}^2)^{11/72} + (\widetilde{M_0} N_0)^{-5/72} (N_0 v_{g0})^{-73/36} (\widetilde{M_2} N_0 v_{g0}^2)^{7/72} \Big) \end{cases}$$

$$\begin{cases} \frac{d\widetilde{M_0}}{d\tau} &= \frac{-B(\tau)}{v_{g0}^{1/6} N_0^2} \left(\widetilde{M_0}^{151/72} \widetilde{M_2}^{19/72} + 2\widetilde{M_0}^{131/72} \widetilde{M_2}^{-1/72} + \widetilde{M_0}^{127/72} \widetilde{M_2}^{-5/72} \right) N_0^2 v_{g0}^{1/6} \\ \frac{d\widetilde{M_2}}{d\tau} &= \frac{2B(\tau)}{v_{g0)}^{11/6} N_0^2} \left(\widetilde{M_0}^{19/72} \widetilde{M_2}^{31/72} + 2\widetilde{M_0}^{-1/72} \widetilde{M_2}^{11/72} + \widetilde{M_0}^{-5/72} \widetilde{M_2}^{7/72} \right) N_0^2 v_{g0}^{11/6} \end{cases}$$

$$\begin{cases} \frac{d\widetilde{M_0}}{d\tau} &= -B(\tau) \left(\widetilde{M_0}^{151/72} \widetilde{M_2}^{19/72} + 2\widetilde{M_0}^{131/72} \widetilde{M_2}^{-1/72} + \widetilde{M_0}^{127/72} \widetilde{M_2}^{-5/72} \right) \\ \frac{d\widetilde{M_2}}{d\tau} &= 2B(\tau) \left(\widetilde{M_0}^{19/72} \widetilde{M_2}^{31/72} + 2\widetilde{M_0}^{-1/72} \widetilde{M_2}^{11/72} + \widetilde{M_0}^{-5/72} \widetilde{M_2}^{7/72} \right) \end{cases} \tag{6.18}$$

BIBLIOGRAPHY

[1] P. Tunved, *An introduction to crossbow hunting,* University Lecture (2000).

[2] T. Kodas and M. Hampden-Smith, *Aerosol Processing of Materials* (Wiley, 1999).

[3] D. J. Rader, *Momentum slip correction factor for small particles in nine common gases,* Journal of Aerosol Science **21**, 161 (1990).

[4] Kaye and Laby, *Tables of physical chemical constants,* (1995).

[5] S. Park, K. Lee, E. Otto, and H. Fissan, *The log-normal size distribution theory of brownian aerosol coagulation for the entire particle size range: Part i—analytical solution using the harmonic mean coagulation kernel,* Journal of Aerosol Science **30**, 3 (1999).

[6] K. W. Lee, J. Chen, and J. A. Gieseke, *Log-normally preserving size distribution for brownian coagulation in the free-molecule regime,* Aerosol Science and Technology **3**, 53 (1984), https://doi.org/10.1080/02786828408958993 .

[7] M. V. Smoluchowski, *Drei Vortrage uber Diffusion, Brownsche Bewegung und Koagulation von Kolloidteilchen,* Zeitschrift fur Physik **17**, 557 (1916).

[8] M. Boeije, *Influencing the nanoparticle generation and deposition process,* (2018).

[9] J. Feng, G. Biskos, and A. Schmidt-Ott, *Toward industrial scale synthesis of ultrapure singlet nanoparticles with controllable sizes in a continuous gas-phase process,* in *Scientific reports* (2015).

[10] W. C. Hinds, *Aerosol technology: Properties, Behavior and Measurement of Airborne Particles.* (1999).

[11] H. Müller, *Zur allgemeinen Theorie ser raschen Koagulation,* Fortschrittsberichte uber Kolloide und Polym. **27**, 223–250 (1928).

[12] M. Yu and L. Yueyan, *Methods of moments for resolving aerosol dynamics,* in *Aerosols - Science and Case Studies*, edited by K. Volkov (InTech, Rijeka, 2016) Chap. 02.

[13] R. N. Sinn, *Dekker Encyclopedia on nanoscience and nanotechnology*, edited by J. A. S. C. I. C. K. Putyera, Vol. 1 A-C 1-892 (Marcel Dekker, Inc., 2004) pp. 36–38.

[14] E. Otto, H. Fissan, S. Park, and K. Lee, *The log-normal size distribution theory of brownian aerosol coagulation for the entire particle size range: part ii—analytical solution using dahneke's coagulation kernel,* Journal of Aerosol Science **30**, 17 (1999).

[15] T. Trzeciak, *Brownian Coagulation at High Particle Concentrations.*, Ph.D. thesis, Delft University of Technology (2012).

[16] P.-I. Au, J. Liu, and Y.-K. Leong, *Yield stress and microstructure of washed oxide suspensions at the isoelectric point: experimental and model fractal structure,* Rheologica Acta **55**, 847 (2016).

[17] E. Newman and K. Kingsley, *An introduction to the method of moments,* Computer Physics Communications **68**, 1 (1991).

[18] P. R. Estrada and J. N. Cuzzi, *Solving the coagulation equation by the moments method,* The Astrophysical Journal **682**, 515 (2008).

[19] G. C. Razvan Tamas, Ana Dumitrascu, *Alternative applications of the method of moments: from electromagnetic waves to source synthesis, deconvolution, and data processing in navigation systems,* (2015).

[20] M. Yu, J. Lin, and T. Chan, *A new moment method for solving the coagulation equation for particles in brownian motion,* Aerosol Science and Technology **42**, 705 (2008), https://doi.org/10.1080/02786820802232972.

[21] M. Kraft, *Modelling of particulate processes,* KONA Powder and Particle Journal **23**, 18 (2005).

[22] M. Yamamoto, *A moment method of the log-normal size distribution with the critical size limit in the free-molecular regime,* Aerosol Science and Technology **48**, 725 (2014), https://doi.org/10.1080/02786826.2014.922161.

[23] M. Frenklach and S. J. Harris, *Aerosol dynamics modeling using the method of moments,* Journal of Colloid and Interface Science **118**, 252 (1987).

[24] J. E. Brockmann, P. H. McMurry, and B. Y. H. Liu, *On simultaneous coagulation and diffusional loss of free molecule aerosols in turbulent pipe flow,* Aerosol Science and Technology **1**, 163 (1982), https://doi.org/10.1080/02786828208958585.

[25] R. R. Zagidullin, A. P. Smirnov, S. A. Matveev, and E. E. Tyrtyshnikov, *An efficient numerical method for a mathematical model of a transport of coagulating particles,* Moscow University Computational Mathematics and Cybernetics **41**, 179 (2017).

[26] V. Smorodin, *Revising the fuchs "boundary sphere" method.* Wagner P.E. (eds) Nucleation and Atmospheric Aerosols (2007).

[27] N. Morgan, *Numerical Modelling of the Growth of Nanoparticles*, Ph.D. thesis, University of Cambridge (2007).

[28] K. W. Lee and H. Chen, *Coagulation rate of polydisperse particles,* Aerosol Science and Technology **3**, 327 (1984), https://doi.org/10.1080/02786828408959020.